Structural and electronic properties of the molecular conductors $(EDTTTF)_x[Pd(dmit)_2]_y$ (x:y=2:3 and 2:2)

1995 J. Phys.: Condens. Matter 7 4673

(http://iopscience.iop.org/0953-8984/7/24/008)

J. Phys.: Condens. Matter 7 (1995) 4673–4695. Printed in the UK

Structural and electronic properties of the molecular conductors (EDTTTF)$_x$[Pd(dmit)$_2$]$_y$ (x:y = 2:3 and 2:2)

M-L Doublet†, E Canadell†, B Garreau§, J-P Legros§, L Brossard‡, P Cassoux§ and J-P Pouget‖

† Laboratoire de Chimie Théorique, Bâtiment 490, Université Paris-Sud, 91405 Orsay, France
‡ Service National des Champs Magnétiques Pulsés et Laboratoire de Physique des Solides, INSA–Université Paul Sabatier de Toulouse, avenue de Rangueil, 31077 Toulouse Cédex, France
§ Laboratoire de Chimie de Coordination du CNRS (UP 8241) lié par convention à l'Université Paul Sabatier, 205 route de Narbonne, 31077 Toulouse Cédex, France
‖ Laboratoire de Physique des Solides associé au CNRS (UA 040002), Bâtiment 510, Université Paris-Sud, 91405 Orsay, France

Received 20 February 1995

Abstract. Two new charge transfer salts combining the EDTTTF (ethylenedithiotetrathiafulvalene) donor and the Pd(dmit)$_2$ acceptor (dmit^{2-} = 4, 5-dimercapto-1, 3-dithiole-2-thione) have been prepared and characterized. The molecular structure of the (EDTTTF)$_2$[Pd(dmit)$_2$]$_3$ salt is quite unusual since the Pd(dmit)$_2$ entities form true trimers through two strong interactions between the Pd atoms. These trimers of acceptors form slabs which alternate with slabs of (EDTTTF)$_2$ pairs. Band structure calculations indicate a charge transfer of one electron per EDTTTF molecule and we expect this 2:3 salt to be a semiconductor. In the (EDTTTF)$_2$[Pd(dmit)$_2$]$_2$ salt, the EDTTTF units form centrosymmetric pairs which pile up along [100] while the [Pd(dmit)$_2$]$_2$ dimers pile up along [101]. Stacks of donors and acceptors form segregated slabs which alternate along [010]. (EDTTTF)$_2$[Pd(dmit)$_2$]$_2$ is metallic, and our studies suggest the occurrence of a charge transfer of $\frac{3}{4}$ electrons per molecule. This salt exhibits a resistivity anomaly, a drop of spin susceptibility and a structural phase transition at 50 K. These data combined with electronic structure calculations show that this transition must be associated with a charge density wave (CDW) instability of the EDTTTF stacks. Finally we suggest that the resistivity anomaly of the related α-(EDTTTF)[Ni(dmit)$_2$] salt is also due to a CDW instability of the donor slabs.

1. Introduction

Up to 1987 most of the research work on molecular conductors involved symmetrical donors such as TTF (tetrathiafulvalene), TMTSF (tetramethyltetraselenafulvalene) or BEDTTTF (bis-ethylenedithiotetrathiafulvalene) and resulted in the synthesis of a large number of conductive phases which display a wide range of electrical behaviours including metallic conductivity and superconductivity [1]. The asymmetrical donors were generally thought to be less suitable because they would not lead to structures with sufficient order to allow for superconductivity. However, several groups succeeded in obtaining conductive (and even superconductive) phases using asymmetrical π-donor molecules such as DMET (dimethylethylenedithiodiselenadithiafulvalene) [2] and MDTTTF (methylenedithiotetrathiafulvalene) [3]. Another asymmetrical donor, EDTTTF (ethylenedithiotetrathiafulvalene, figure 1(a)) was reported to give a series of phases with interesting conductivity properties. The cation radical salts (EDTTTF)$_2$X (X =

0953-8984/95/244673+23$19.50

$AuBr_2^-$, AuI_2^-, PF_6^-, TaF_6^-, ClO_4^-, BF_4^-, ...) [4–5] display a metal-like conductivity in the high-temperature range and $(EDTTTF)_2IBr_2$ remains metallic down to very low temperature [4].

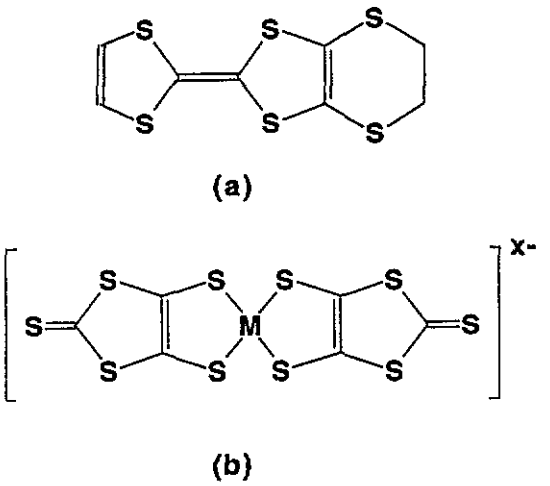

Figure 1. The EDTTTF (a) and M(dmit)$_2$ (b) molecules (M = Ni, Pd, Pt).

On the other hand, the metal complexes M(dmit)$_2$ (M = Ni, Pd, Pt and dmit = 4, 5-dimercapto-1, 3-dithiole-2-thione†, figure 1(b)) are known to play the role of electron acceptors with non-integer oxidation states, yielding highly conducting and even superconducting (under pressure) systems, when associated with either donor molecules (such as TTF) or closed-shell cations (organic, such as NR_4^+ with R = Me, Et, ..., or inorganic, such as $Cs,^+$ ...) [6].

Systems resulting from the combination of the symmetrical acceptors M(dmit)$_2$ with asymmetrical donors are expected to afford interesting transport properties. Actually, two allotropic forms (α and β) of the charge transfer complex (EDTTTF)[Ni(dmit)$_2$] have been characterized [7]: The β-form is a semiconductor while the α-form remains metallic down to very low temperature and becomes superconductive ($T_c \simeq 1.3$ K) at ambient pressure [8]. Substitution of Pd for Ni as the metal M of the acceptor M(dmit)$_2$ has yielded two phases $(EDTTTF)_2[Pd(dmit)_2]_3$ and $(EDTTTF)_2[Pd(dmit)_2]_2$ [9]. The latter remains metallic down to 500 mK and displays a temperature dependence of the conductivity similar to that of α-(EDTTTF)[Ni(dmit)$_2$]; however it does not become superconductive even under pressure [10].

As part of a current research work which aims to rationalize the transport properties of molecular conductors derived from metal–dmit complexes [11–18], this paper reports on the crystal and electronic structures of the two phases $(EDTTTF)_x[Pd(dmit)_2]_y$ ($x : y = 2:3$ and 2:2). Following the preliminary investigations of [10] and [19], the electrical and magnetic properties and the low-temperature x-ray scattering study of the 2:2 phase are also reported.

2. Preparation and characterization

$(EDTTTF)_2[Pd(dmit)_2]_2$ and $(EDTTTF)_2[Pd(dmit)_2]_3$ were obtained simultaneously by galvanostatic electrolysis of an acetonitrile solution (60 ml) of $(n\text{-}NBu_4)[Pd(dmit)_2]$

† Or 2-thioxo-1, 3-dithiole- 4, 5-dithiolato.

Table 1. Non-hydrogen atom fractional coordinates and equivalent isotropic temperature factors for (EDTTTF)$_2$[Pd(dmit)$_2$]$_3$ with estimated standard deviations in parentheses.

Atom	*x/a*	*y/b*	*z/c*	*B* (Å^2)
Pd(1)	0.500	0.500	0.500	2.37(2)
S(11)	0.6278(2)	0.4874(2)	0.3491(3)	2.70(5)
S(12)	0.8271(2)	0.6182(2)	0.3954(3)	3.04(5)
S(13)	0.9907(2)	0.7887(2)	0.5759(4)	4.98(7)
S(14)	0.8083(2)	0.7439(2)	0.7116(3)	3.16(5)
S(15)	0.6044(2)	0.6316(2)	0.7015(3)	2.71(5)
C(11)	0.7170(7)	0.5868(6)	0.464(1)	2.4(2)[a]
C(12)	0.8817(7)	0.7200(6)	0.562(1)	3.0(2)[a]
C(13)	0.7071(6)	0.6476(6)	0.617(1)	2.3(2)[a]
Pd(2)	0.403 85(5)	0.628 18(4)	0.260 84(8)	1.96(1)
S(21)	0.5191(2)	0.6243(2)	0.0906(3)	2.54(5)
S(22)	0.7188(2)	0.7610(2)	0.1326(3)	2.54(5)
S(23)	0.8682(2)	0.9458(2)	0.2944(3)	3.68(6)
S(24)	0.6944(2)	0.8894(2)	0.4385(3)	2.83(5)
S(25)	0.4963(2)	0.7709(2)	0.4405(3)	2.65(5)
S(26)	0.2992(2)	0.4906(2)	0.0735(3)	2.55(5)
S(27)	0.0791(2)	0.4049(2)	0.0452(3)	3.00(6)
S(28)	−0.1165(2)	0.3869(2)	0.1654(4)	4.54(7)
S(29)	0.0664(2)	0.5369(2)	0.3606(3)	2.97(5)
S(30)	0.2843(2)	0.6394(2)	0.4262(3)	2.56(5)
C(21)	0.6097(6)	0.7263(6)	0.205(1)	2.0(2)[a]
C(22)	0.7675(6)	0.8693(6)	0.290(1)	2.6(2)[a]
C(23)	0.5986(6)	0.7860(5)	0.3496(9)	1.9(2)[a]
C(24)	0.1902(6)	0.4902(6)	0.151(1)	2.1(2)[a]
C(25)	0.0037(7)	0.4392(6)	0.189(1)	3.0(2)[a]
C(26)	0.1842(6)	0.5522(6)	0.302(1)	2.1(2)[a]
S(1)	0.4671(2)	0.8040(2)	0.9164(3)	3.00(5)
S(2)	0.3423(2)	0.9119(2)	0.7361(3)	3.29(6)
S(3)	0.6765(2)	0.9291(2)	0.9146(3)	2.80(5)
S(4)	0.5600(2)	1.0395(2)	0.7298(3)	2.55(5)
S(5)	0.8840(2)	1.0293(2)	0.9410(4)	4.80(7)
S(6)	0.7456(2)	1.1650(2)	0.7187(3)	3.39(6)
C(1)	0.3338(7)	0.7728(6)	0.871(1)	3.3(2)[a]
C(2)	0.2783(7)	0.8219(7)	0.792(1)	3.5(2)[a]
C(3)	0.7492(6)	1.0186(6)	0.868(1)	2.5(2)[a]
C(4)	0.6952(6)	1.0695(6)	0.783(1)	2.3(2)[a]
C(5)	0.9300(7)	1.1417(6)	0.914(1)	3.6(2)[a]
C(6)	0.8825(8)	1.1524(7)	0.747(1)	4.3(2)[a]
C(7)	0.4652(6)	0.8963(6)	0.825(1)	2.2(2)[a]
C(8)	0.5564(6)	0.9490(6)	0.821(1)	2.3(2)[a]

[a] Refined isotropically.

(44.03 mg, 0.059 mmol) and EDTTTF (9.73 mg, 0.033 mmol) carried out in a nitrogen-flushed U-type cell where the anodic and cathodic compartments were separated by a medium-porosity glass frit. Platinum electrodes were used. The cell was thermostated (20 °C) and the current ($I = 1$ μA, current density $= 1.6 \times 10^{-6}$A cm^{-2}) was held constant. After three weeks black platelets formed on the anode and were collected by filtration, washed with acetonitrile and vacuum-dried.

Two phases of stoichiometry 2:2 and 2:3 were identified, the stoichiometry of these phases was deduced from the x-ray study (vide infra). Actually, only one crystal of the 2:3

phase was isolated by chance; no other crystal of this phase could be sorted out. All crystals used for subsequent physical studies were thus routinely checked for their cell parameters; all of them were the 2:2 phase.

3. Crystal structures

Intensity data were collected at room temperature on an Enraf–Nonius automatic four-circle diffractometer using monochromatized Mo Kα ($\lambda = 0.7107$ Å) radiation and ω–2θ scan mode with variable-speed technique. The structures were solved by direct methods [20] and refined by standard full-matrix least-squares and Fourier procedures [21]. All hydrogen atoms were located on Fourier difference maps and introduced in idealized positions ($d_{C-H} = 0.95$ Å) with arbitrary isotropic temperature factors $U = 0.05$ Å^2.

3.1. (EDTTTF)$_2$[Pd(dmit)$_2$]$_3$

Triclinic, $P\bar{1}, a = 13.210(2), b = 14.687(2), c = 8.528(1)$ Å, $\alpha = 105.84(2), \beta = 101.36(2), \gamma = 95.87(1)°, V = 1539.1(7)$ Å^3, $Z = 1$ for $C_{34}H_{12}Pd_3S_{42}$, $\mu = 22.6$ cm^{-1}. Out of the 2536 independent reflections measured in the range $2 \leqslant \theta \leqslant 20°$, 1931 having $|F_0| > 2\sigma(|F_0|)$ were considered observed and used in the calculations. The palladium and sulphur atoms were assigned anisotropic temperature factors, the carbon atoms being refined with isotropic temperature factors. Final R and R_w values were 0.027 and 0.031 for 273 variable parameters. Non-hydrogen atom coordinates are given in table 1; atoms are labelled according to figure 2.

The molecular structure shows a somewhat unusual feature: the Pd(dmit)$_2$ entities form true chemical trimers through two strong interactions between the palladium atoms; the Pd–Pd distance is 3.30 Å (figure 3(a)). In a trimer the three Pd(dmit)$_2$ entities are fully eclipsed; the occurrence of the strong Pd–Pd interactions is demonstrated by the planarity of the central centrosymmetric entity while the external ones are bent because of sulphur–sulphur repulsions (the angle between the two dmit mean planes of an external Pd(dmit)$_2$ unit is 14°). Such an association of three Pd(dmit)$_2$ molecules has never been reported before.

In contrast with the neutral EDTTTF molecule (figure 4(a)) [9, 22], the oxidized EDTTTF unit in this compound is planar except, of course, for the ethylenic residue (figure 4(b)). Figure 5 shows a part of the crystal packing. Slabs of EDTTTF entities, parallel to (010), alternate along the [010] direction with slabs of [Pd(dmit)$_2$]$_3$ trimers. The slabs of the donor are built of columns parallel to [001], made of centrosymmetric dimers which show an eclipsed overlap of the TTF moieties (figure 6). The distance between the mean planes of the two molecules of a dimer is 3.325 Å. The molecular planes are not perpendicular to [001]: the longitudinal molecular axis makes an angle of 70° with the stacking direction and the transverse molecular axis makes an angle of 52° with the stacking direction; as a result, two EDTTTF molecules which belong to two adjacent dimers do not overlap. Within an acceptor slab the [Pd(dmit)$_2$]$_3$ trimers lie side by side. The mean molecular plane of the acceptor is almost perpendicular (90.5°) to that of the donor. Details of the shortest (<3.7 Å) intermolecular sulphur-to-sulphur contacts are shown in table 2.

3.2. (EDTTTF)$_2$[Pd(dmit)$_2$]$_2$

Triclinic, $P\bar{1}, a = 7.595(1), b = 26.952(4), c = 6.453(3)$ Å, $\alpha = 93.11(3), \beta = 111.19(2), \gamma = 91.75(1)°, V = 1228.0(7)$ Å^3, $Z = 2$ for $C_{14}H_6PdS_{16}$, $\mu = 20.8$ cm^{-1}.

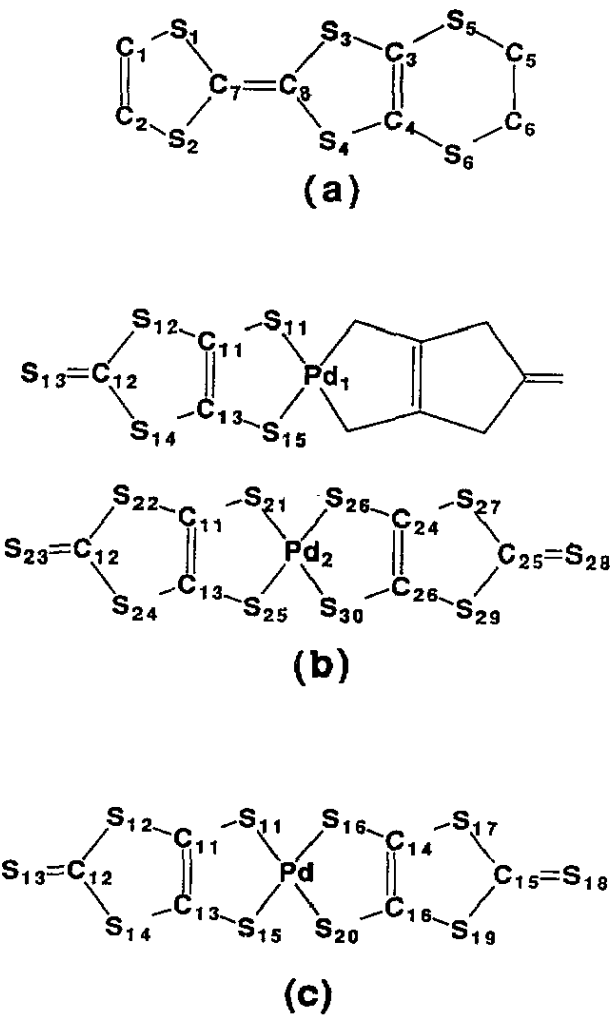

Figure 2. Atom numbering used for the x-ray diffraction study of (EDTTTF)$_2$[Pd(dmit)$_2$]$_3$ (a, b) and (EDTTTF)$_2$[Pd(dmit)$_2$]$_2$ (a, c).

Out of the 3420 independent reflections measured in the range $2 \leqslant \theta \leqslant 23°$, 2730 having $|F_0| > 2\sigma(|F_0|)$, were considered observed and used in the calculations. All non-hydrogen atoms were refined using anisotropic temperature factors. Final R and R_w values were 0.023 and 0.030 for 298 variable parameters. Non-hydrogen atom coordinates are given in table 3; atoms are labelled according to figure 2.

As usually observed in most of the previously studied palladium complexes with the dmit ligand [12, 23–25], the Pd(dmit)$_2$ molecules are paired through a strong interaction between the palladium atoms†; the Pd–Pd distance is 3.09 Å (figure 3(b)). The two units forming the dimer are fully eclipsed, which results in a central bending of the Pd(dmit)$_2$ units due to the sulphur–sulphur repulsions (the angle between the mean dmit planes is 6°). In contrast to the 2:3 phase the oxidized EDTTTF species is not planar and displays a boat conformation: the dihedral angles between the mean planes defined by the atoms S(1), S(2),

† This is the reason for writing (EDTTTF)$_2$[Pd(dmit)$_2$]$_2$ instead of (EDTTTF)[Pd(dmit)$_2$].

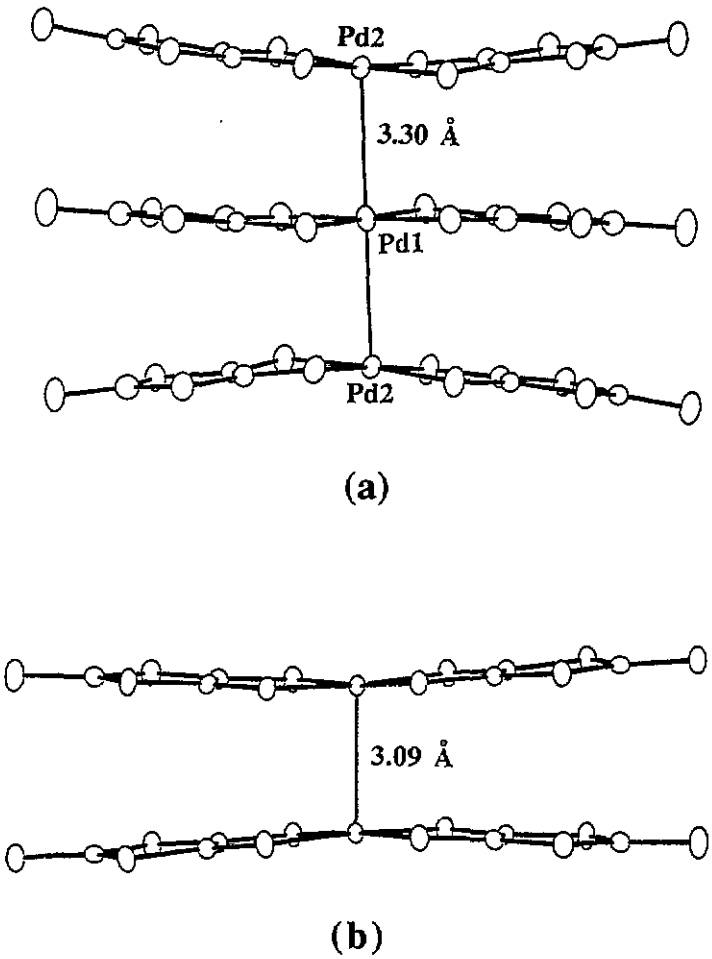

Figure 3. Side view of the $[Pd(dmit)_2]_3$ trimers (a) in $(EDTTTF)_2[Pd(dmit)_2]_3$ and $[Pd(dmit)_2]_2$ dimers (b) in $(EDTTTF)_2[Pd(dmit)_2]_2$.

S(3), S(4), C(7), C(8) on the one hand and S(1), S(2), C(1), C(2) and S(3), S(4), C(3), C(4), S(5), S(6) on the other hand are 3° and 10° respectively (figure 4(c)).

Figure 7 shows the molecular packing of $(EDTTTF)_2[Pd(dmit)_2]_2$: the EDTTTF units form centrosymmetric pairs which pile up along [100] while the $[Pd(dmit)_2]_2$ dimers pile up along [101] (figure 8). The adjacent stacks of the donor and of the acceptor form slabs parallel to (010) which alternate along [010]. Details of the shortest (<3.7 Å) intermolecular sulphur-to-sulphur contacts are shown in table 4.

To some extent the parent compound α-(EDTTTF)[Ni(dmit)$_2$] displays a similar structure with different stacking directions for the donor and acceptor molecules [7] and similar modes of overlap for the donor molecules (figure 9). However an important difference lies in the relative positions of the M(dmit)$_2$ entities, which lead to quite different structures for the anionic stacks. The strong dimerization of the Pd(dmit)$_2$ anions in $(EDTTTF)_2[Pd(dmit)_2]_2$ results in an eclipsed intradimer overlap alternating with an interdimer overlap characterized by a longitudinal and transverse offset (figure 10(a)). In contrast, the Ni(dmit)$_2$ anions in α-(EDTTTF)[Ni(dmit)$_2$] form regular stacks in which they are slipped sideways (figure 10(b)).

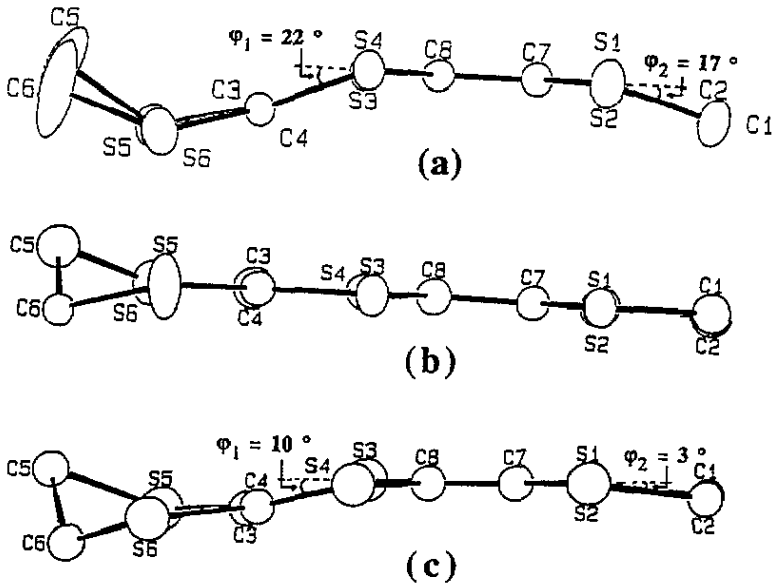

Figure 4. Side view of the EDTTTF molecule in neutral EDTTTF (a), $(EDTTTF)_2[Pd(dmit)_2]_3$ (b) and $(EDTTTF)_2[Pd(dmit)_2]_2$ (c).

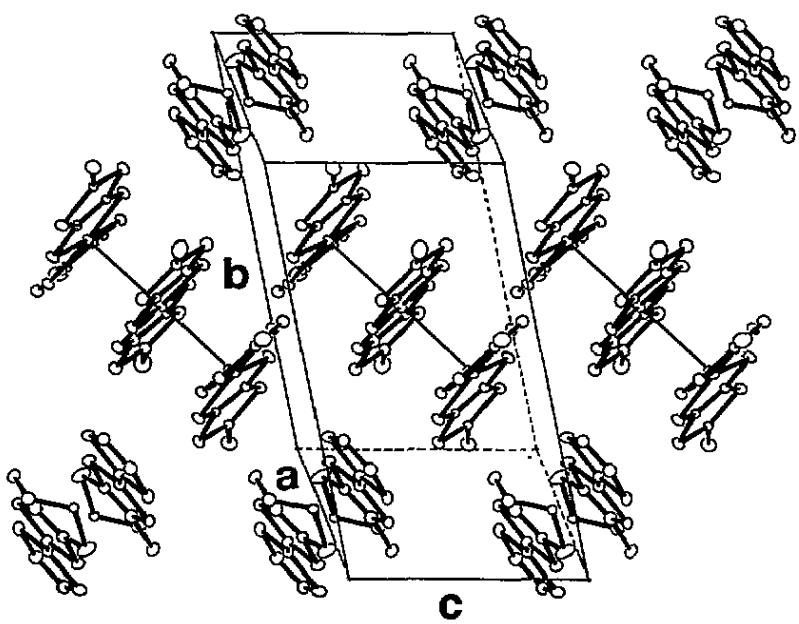

Figure 5. Crystal packing of $(EDTTTF)_2[Pd(dmit)_2]_3$.

This has important consequences for the electronic structure, which will be discussed in the next section.

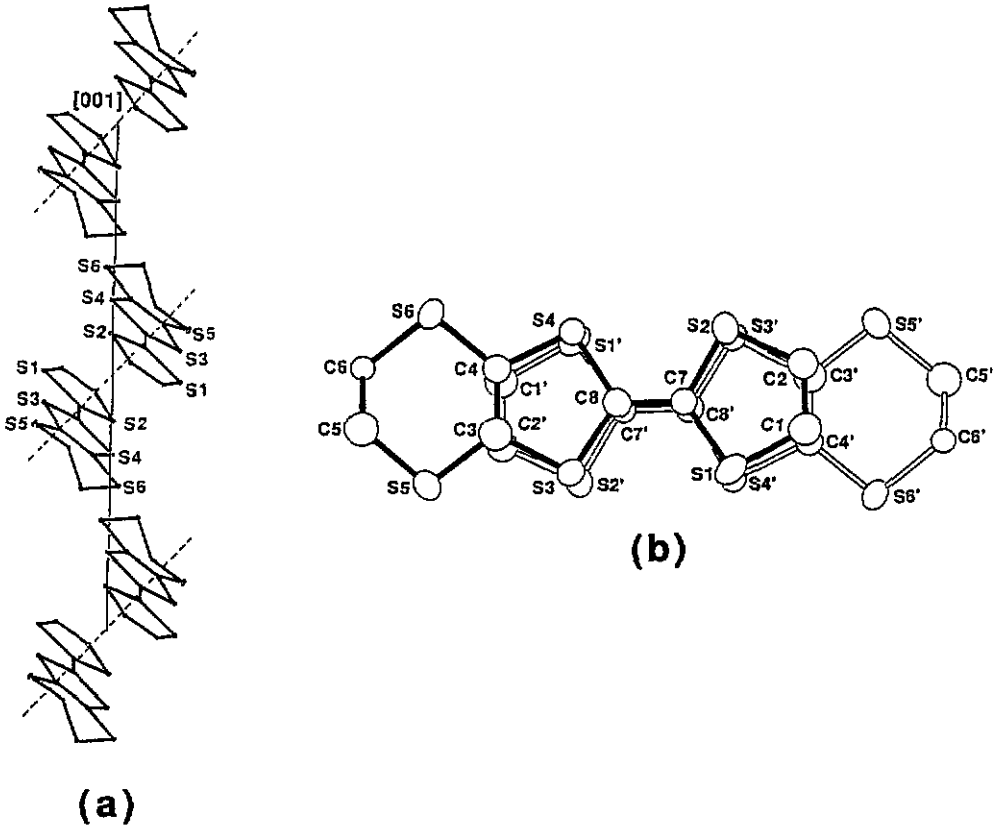

Figure 6. Stacking mode (a) and mode of overlap of the EDTTTF molecules within a centrosymmetric dimer (b) in (EDTTTF)$_2$[Pd(dmit)$_2$]$_3$; primed labels refer to the 'white' molecule.

4. Electronic structure

The physical properties of several M(dmit)$_2$ (M = Ni, Pd, Pt) charge transfer salts have been quite successfully rationalized on the basis of tight-binding extended Hückel type calculations [11–14, 16–17]. A previous study of Cs[Pd(dmit)$_2$]$_2$ [12] proved that the main features of the band structure and Fermi surface of this salt were independent of the use of single-ζ or double-ζ Slater-type orbitals. Thus, in order to correlate the crystal structure (section 3) and the transport properties (section 5) of (EDTTTF)$_2$[Pd(dmit)$_2$]$_3$ and (EDTTTF)$_2$[Pd(dmit)$_2$]$_2$ we decided to carry out a single-ζ tight-binding extended Hückel study [26] of their electronic structures and to compare the results for the 2:2 salt with those of the parent compound α-(EDTTTF)[Ni(dmit)$_2$]. The exponents and parameters used in our calculations were taken from previous work [17]. The weighted Wolfsberg–Helmholz formula was used in the calculation of the non-diagonal matrix elements of the Hamiltonian [27].

4.1. (EDTTTF)$_2$[Pd(dmit)$_2$]$_3$

The calculated band structures for the EDTTTF and Pd(dmit)$_2$ slabs of (EDTTTF)$_2$[Pd(dmit)$_2$]$_3$ are shown in figures 11(a) and 11(b), respectively. The unit cell of the donor slabs contains

Table 2. Intermolecular S...S distances (Å) less than 3.7 Å in (EDTTTF)$_2$[Pd(dmit)$_2$]$_3$.

Atom 1	Atom 2	Distance	Symmetry operation for atom 2
donor...donor			
S(1)	S(4)	3.362(3)	$1-x, 2-y, 2-z$
S(2)	S(3)	3.319(4)	$1-x, 2-y, 2-z$
S(2)	S(6)	3.639(4)	$1-x, 2-y, 1-z$
S(5)	S(5)	3.309(3)	$2-x, 2-y, 2-z$
donor...acceptor			
S(1)	S(15)	3.576(3)	x, y, z
S(1)	S(21)	3.432(4)	$x, y, 1+z$
S(1)	S(22)	3.674(3)	$x, y, 1+z$
S(2)	S(23)	3.660(4)	$1-x, 2-y, 1-z$
S(2)	S(24)	3.656(4)	$1-x, 2-y, 1-z$
S(3)	S(14)	3.606(3)	x, y, z
S(3)	S(22)	3.501(4)	$x, y, 1+z$
S(3)	S(23)	3.631(3)	$x, y, 1+z$
S(4)	S(25)	3.555(4)	$1-x, 2-y, 1-z$
S(5)	S(23)	3.586(5)	$x, y, 1+z$
S(6)	S(25)	3.543(4)	$1-x, 2-y, 1-z$
S(6)	S(30)	3.453(4)	$1-x, 2-y, 1-z$
acceptor...acceptor			
intratrimer			
S(11)	S(21)	3.565(4)	x, y, z
S(12)	S(22)	3.657(4)	x, y, z
S(12)	S(29)	3.689(4)	$1-x, 1-y, 1-z$
S(14)	S(27)	3.635(4)	$1-x, 1-y, 1-z$
S(15)	S(25)	3.604(4)	x, y, z
intertrimer			
S(11)	S(21)	3.694(3)	$1-x, 1-y, -z$
S(12)	S(28)	3.660(4)	$1+x, y, z$
S(12)	S(29)	3.528(4)	$1+x, y, z$
S(15)	S(22)	3.583(3)	$x, y, 1+z$
S(21)	S(21)	3.492(3)	$1-x, 1-y, -z$
S(21)	S(26)	3.380(3)	$1-x, 1-y, -z$
S(22)	S(26)	3.597(3)	$1-x, 1-y, -z$
S(29)	S(29)	3.547(4)	$-x, 1-y, 1-z$

two molecules so that the band structure of figure 11(a) contains two bands built from the two EDTTTF HOMOs (highest occupied molecular orbitals). The unit cell of the acceptor slabs contains a trimeric [Pd(dmit)$_2$]$_3$ unit. In addition, since the HOMO and LUMO (lowest unoccupied molecular orbital) of Pd(dmit)$_2$ are quite close in energy (~0.4 eV according to the single-ζ calculations), the band structure of figure 11(b) contains three HOMO and three LUMO bands. As is the case for the slabs containing [Pd(dmit)$_2$]$_2$ dimers [11–14] there is no net separation between the HOMO and LUMO bands. In fact two of the LUMO bands stay lower in energy than the higher HOMO band. The essential features of figure 11(b) are that all the bands are very flat and that there is a clear energy gap between the fourth and fifth bands from the bottom. This suggests that (a) the acceptor slabs should not be the main contributors to the conductivity of this salt and (b) the oxidation state of the trimeric units should be [Pd(dmit)$_2$]$_3^{2-}$. As described in section 3.1, the asymmetrical nature of EDTTTF leads to the presence of dimeric units with four short S···S interactions (see figure 6(b) and table 2). The eclipsed overlap of the two TTF moieties leads to a very strong $\beta_{\text{HOMO-HOMO}}$ interaction energy (0.72 eV) [28]. These dimers form chains along the

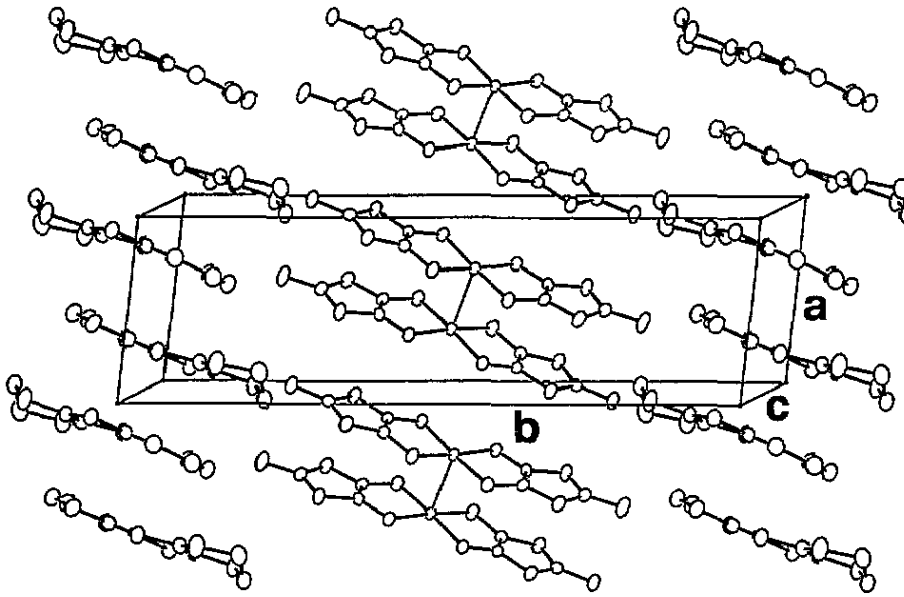

Figure 7. Crystal packing of (EDTTTF)$_2$[Pd(dmit)$_2$]$_2$.

c direction and are arranged in such a way that the contacts between the successive dimers are through the sulphur atoms of the outer six-membered rings (see figure 6(a)). Since, as in BEDTTTF [28], the contributions of the outer sulphur atoms to the HOMO are only about one-third of those of the inner sulphur atoms, the $\beta_{\text{HOMO-HOMO}}$ interaction energy along the *c* direction is non-negligible but small (0.12 eV). The interaction energies along the other directions of the slab are all extremely small. Thus the band structure of figure 11(a) exhibits two strongly split HOMO bands with a dispersion that is relatively weak and only along the *c* direction. The strong band splitting suggests that the upper HOMO band is empty in agreement with the proposed −2 oxidation state for the [Pd(dmit)$_2$]$_3$ trimeric units. Thus we believe that the EDTTTF donors in (EDTTTF)$_2$[Pd(dmit)$_2$]$_3$ are in a +1 oxidation state and that the temperature dependence of the conductivity of this salt should be of the semiconducting type.

4.2. *(EDTTTF)$_2$[Pd(dmit)$_2$]$_2$*

The calculated band structures for the EDTTTF and Pd(dmit)$_2$ layers of (EDTTTF)$_2$[Pd(dmit)$_2$]$_2$ are shown in figures 12(a) and 12(b), respectively. Let us recall that the EDTTTF donors and the Pd(dmit)$_2$ acceptors pile up along the *a* and $(a + c)$ directions, respectively. Since the charge transfer in (EDTTTF)$_2$[Pd(dmit)$_2$]$_2$ is not known, we have reported in figure 12 the Fermi levels appropriate for different electron transfers: $\frac{1}{2}$ (ε_F), $\frac{3}{4}$(ε'_F) and one (ε''_F) electrons per molecule. The two EDTTTF HOMO bands are quite dispersive along a^* and practically coincide at the X point. This means that although the two interactions along the chains are geometrically different, from the electronic viewpoint they are very similar. The higher HOMO band is also quite dispersive along the interstack direction so that the Fermi surfaces will be closed for many electron counts. It should be remarked that the two HOMO bands overlap so that the EDTTTF slabs should be metallic whatever the electron transfer.

As discussed in section 3.2, the Pd(dmit)$_2$ units of the acceptor slabs are strongly

Table 3. Non-hydrogen atom fractional coordinates and equivalent isotropic temperature factors for (EDTTTF)$_2$[Pd(dmit)$_2$]$_2$ with estimated standard deviations in parentheses.

Atom	*x/a*	*y/b*	*z/c*	*B* (Å^2)
Pd	0.320 01(3)	0.523 69(1)	0.348 32(4)	1.795(6)
S(11)	0.1462(1)	0.461 47(3)	0.4274(1)	2.21(2)
S(12)	−0.0259(1)	0.364 55(4)	0.1832(2)	2.55(2)
S(13)	−0.1239(2)	0.287 99(4)	−0.1923(2)	3.38(2)
S(14)	0.0850(1)	0.382 86(4)	−0.1925(2)	2.63(2)
S(15)	0.2861(1)	0.480 57(4)	0.0170(2)	2.49(2)
S(16)	0.3293(1)	0.568 32(3)	0.6669(1)	2.19(2)
S(17)	0.4751(1)	0.672 20(4)	0.8474(2)	2.84(2)
S(18)	0.6658(2)	0.769 45(4)	0.8527(2)	4.28(3)
S(19)	0.6019(1)	0.691 11(4)	0.4857(2)	2.87(2)
S(20)	0.4746(1)	0.589 51(4)	0.2605(2)	2.46(2)
C(11)	0.1006(4)	0.4207(1)	0.2040(6)	1.83(7)
C(12)	−0.0260(5)	0.3421(1)	−0.0735(6)	2.28(8)
C(13)	0.1564(5)	0.4294(1)	0.0249(6)	2.00(8)
C(14)	0.4374(5)	0.6228(1)	0.6483(6)	1.92(7)
C(15)	0.5847(5)	0.7141(1)	0.7336(6)	2.63(9)
C(16)	0.4964(5)	0.6322(1)	0.4731(6)	2.12(8)
S(1)	0.2520(2)	1.049 04(4)	0.2323(2)	3.30(2)
S(2)	0.3943(2)	1.071 96(4)	0.7163(2)	3.19(2)
S(3)	0.1074(1)	0.940 14(4)	0.2916(2)	2.80(2)
S(4)	0.2506(1)	0.960 11(4)	0.7776(2)	2.81(2)
S(5)	0.0153(2)	0.833 88(4)	0.2965(2)	4.01(3)
S(6)	0.1982(2)	0.857 44(4)	0.8792(2)	4.39(3)
C(1)	0.3687(6)	1.1066(2)	0.3317(7)	3.8(1)
C(2)	0.4322(6)	1.1170(2)	0.5509(8)	3.8(1)
C(3)	0.1100(5)	0.8895(1)	0.4527(6)	2.60(8)
C(4)	0.1774(5)	0.8985(2)	0.6743(6)	2.74(9)
C(5)	−0.0407(6)	0.8008(2)	0.5037(7)	3.8(1)
C(6)	0.1299(6)	0.7981(2)	0.7179(8)	4.2(1)
C(7)	0.2821(5)	1.0286(1)	0.4934(6)	2.51(9)
C(8)	0.2221(5)	0.9824(1)	0.5191(6)	2.30(8)

dimerized. As usual in M(dmit)$_2$ salts with strong dimerization [11–14], the lowest combination of the two Pd(dmit)$_2$ LUMOs (Ψ^+_{LUMO}) is lower in energy than the highest combination of the two Pd(dmit)$_2$ HOMOs (Ψ^-_{HOMO}) because the strong dimerization leads to a large splitting of each orbital pair which overcomes the initial HOMO–LUMO gap. As shown in figure 12(b), the intermolecular interactions within the slabs do not change this level ordering so that the third band from bottom is the Ψ^-_{HOMO} band. Since Pd(dmit)$_2$ acts as an acceptor and there are two Pd(dmit)$_2$ units per repeat unit of the slab, for any plausible electron transfer (i.e. between zero and one electrons per molecule), the Ψ^-_{HOMO} band will be partially filled. Thus, the partially filled levels of both the donor (EDTTTF) and the acceptor [Pd(dmit)$_2$] partners in this salt are built from the HOMO of the monomeric units.

Because the charge transfer (ρ) in (EDTTTF)$_2$[Pd(dmit)$_2$]$_2$ is not known, we have calculated the Fermi surfaces for both slabs as a function of ρ. Those for the values of $\frac{1}{4}$, $\frac{1}{2}$, $\frac{3}{4}$ and one electron per molecule are shown in figures 13(a), 13(b), 13(c) and 13(d), respectively. The full and dashed lines in these figures correspond to the Fermi surface of the EDTTTF and Pd(dmit)$_2$ slabs, respectively. The Fermi surface of the EDTTTF slabs is

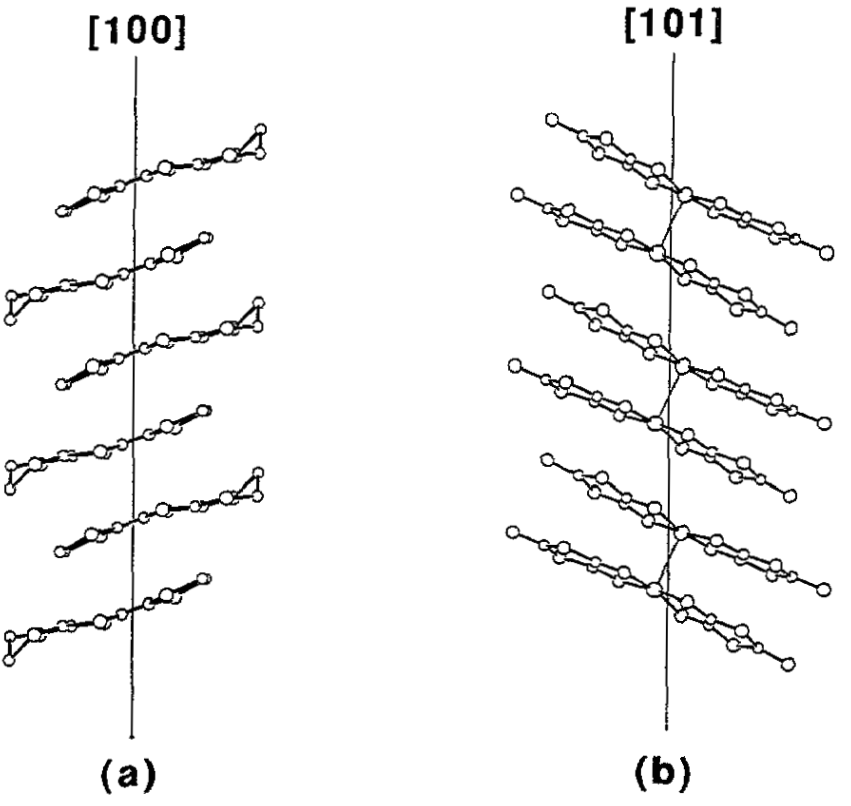

Figure 8. Side view of the stacks of EDTTTF molecules (a) and $[Pd(dmit)_2]_2$ dimers (b) in $(EDTTTF)_2[Pd(dmit)_2]_2$. The plane of the picture is defined by the stacking axis and the longest molecular axis.

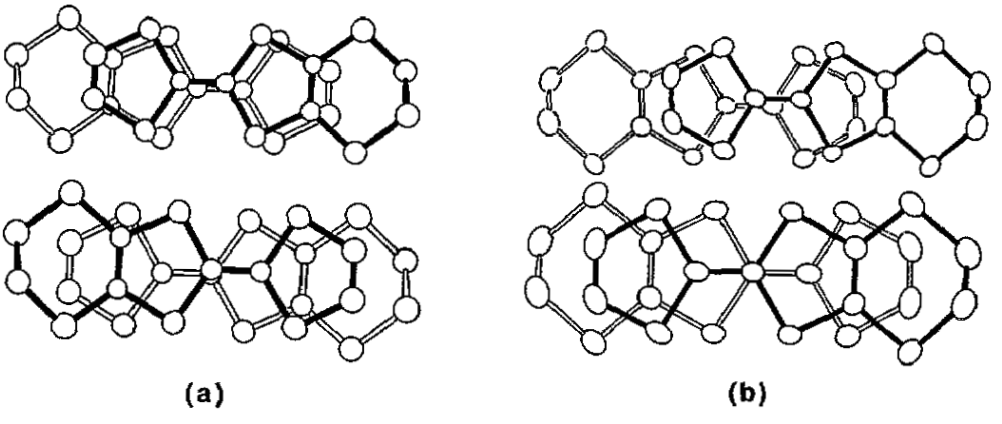

Figure 9. Comparison of the modes of overlap of the EDTTTF molecules in α-$(EDTTTF)[Ni(dmit)_2]$ (a) and $(EDTTTF)_2[Pd(dmit)_2]_2$ (b): intradimer (top) and interdimer (bottom).

closed for small electron transfers, becomes open for larger electron transfers (between 0.6 and 0.8 electrons per molecule) and then closes again. The Fermi surface of the $Pd(dmit)_2$ slabs is also closed for small and large values of ρ but becomes open for values around $\frac{1}{2}$.

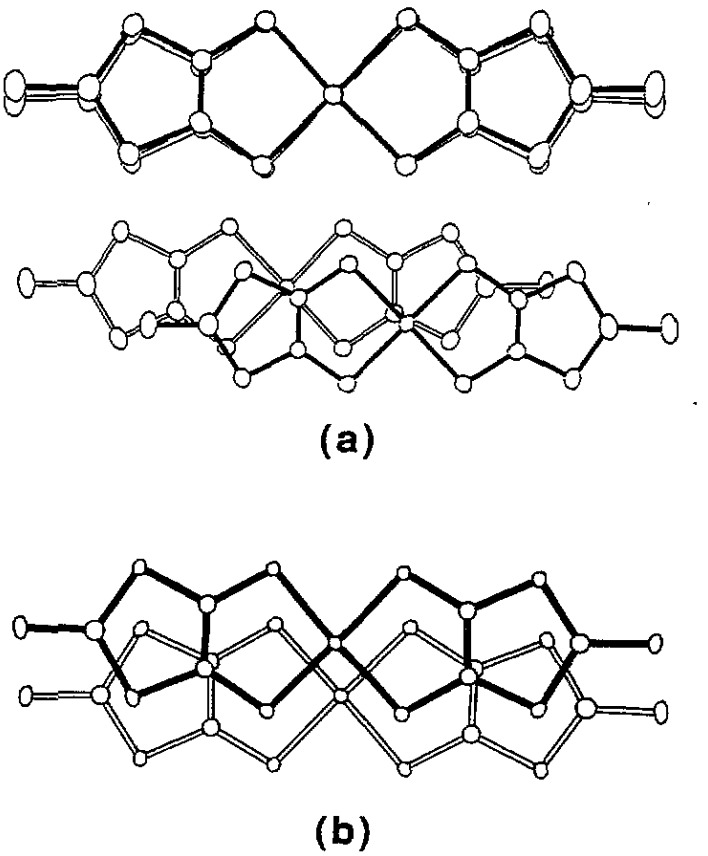

Figure 10. Comparison of the modes of overlap of the M(dmit)$_2$ entities in (EDTTTF)$_2$[Pd(dmit)$_2$]$_2$ (a) and α-(EDTTTF)[Ni(dmit)$_2$] (b).

For $\rho = 1$ the Ψ^-_{HOMO} band is completely filled and the acceptor slabs do not contribute to the Fermi surface. Some of these Fermi surfaces possess nesting vectors which could be at the origin of the resistivity anomaly of (EDTTTF)$_2$[Pd(dmit)$_2$]$_2$. This point will be discussed in detail in the last section of this work.

4.3. α-(EDTTTF)[Ni(dmit)$_2$]

As mentioned in section 3.2, although the crystal structures of the two salts (EDTTTF)$_2$[Pd(dmit)$_2$]$_2$ and α-(EDTTTF)[Ni(dmit)$_2$] are similar, they exhibit some interesting differences. Since both salts exhibit a resistivity anomaly at low temperature, we thought that a comparison of the electronic structures of the two salts could provide some clue to understand the origin of such anomaly. Although a complete study has been carried out [29], we only report here the results relevant for the subsequent discussion.

The main difference between the two crystal structures deals with the structure of the acceptor M(dmit)$_2$ slabs. The unit cell of the Pd(dmit)$_2$ slabs contains two identical and strongly dimerized M(dmit)$_2$ units. In contrast, the unit cell of the Ni(dmit)$_2$ slabs contains two slightly different but non-dimerized M(dmit)$_2$ units. As we have shown elsewhere [14], for non-strongly-dimerized M(dmit)$_2$ systems there is usually no inversion between

Table 4. Intermolecular S...S distances (Å) less than 3.7 Å in (EDTTTF)$_2$[Pd(dmit)$_2$]$_2$.

Atom 1	Atom 2	Distance	Symmetry operation for atom 2
donor...donor			
S(1)	S(3)	3.529(2)	$-x, 2-y, -z$
S(1)	S(4)	3.683(2)	$x, y, -1+z$
S(2	S(4)	3.573(2)	$1-x, 2-y, 2-z$
S(2)	S(6)	3.644(2)	$1-x, 2-y, 2-z$
S(3)	S(6)	3.648(2)	$x, y, -1+z$
S(5)	S(6)	3.524(2)	$x, y, -1+z$
donor...acceptor			
S(5)	S(13)	3.500(2)	$-x, 1-y, -z$
S(5)	S(18)	3.457(5)	$-1+x, y, -1+z$
acceptor...acceptor			
intradimer			
S(11)	S(20)	3.254(5)	$1-x, 1-y, 1-z$
S(12)	S(19)	3.585(5)	$1-x, 1-y, 1-z$
S(14)	S(17)	3.689(5)	$1-x, 1-y, 1-z$
S(15)	S(16)	3.263(6)	$1-x, 1-y, 1-z$
interdimer			
S(11)	S(11)	3.420(3)	$-x, 1-y, 1-z$
S(11)	S(14)	3.472(2)	$x, y, 1+z$
S(11)	S(15)	3.563(5)	$x, y, 1+z$
S(11)	S(16)	3.498(5)	$-x, y, 1+z$
S(12)	S(16)	3.346(5)	$-x, 1-y, 1-z$
S(12)	S(17)	3.457(5)	$-x, 1-y, 1-z$
S(13)	S(19)	3.515(5)	$-x, 1-y, -z$
S(14)	S(16)	3.515(5)	$-x, 1-y, -z$
S(15)	S(15)	3.469(9)	$1-x, 1-y, -z$
S(15)	S(16)	3.445(7)	$x, y, -1+z$
S(15)	S(20)	3.503(6)	$1-x, 1-y, -z$
S(16)	S(20)	3.589(7)	$x, y, 1+z$
S(17)	S(20)	3.567(6)	$x, y, 1+z$

the Ψ^{+}_{LUMO} and Ψ^{-}_{HOMO} levels. However, since the Ni$\cdots$Ni interactions are weak, it is very easy to shift slightly these two levels by changing the nature of the anions. The calculated band structure for the Ni(dmit)$_2$ slabs of α-(EDTTTF)[Ni(dmit)$_2$] is shown in figure 14. (Note that because of the different choice of the crystallographic axes used for α-(EDTTTF)[Ni(dmit)$_2$] [7] the Ni(dmit)$_2$ acceptors pile up along the b direction whereas the EDTTTF donors pile up along the $(a+b)$ direction.) In this case the Ψ^{+}_{LUMO} and Ψ^{-}_{HOMO} bands appear at the same energy region and undergo several avoided crossings (indicated with dots in figure 14). As a result, the partially filled band of the Ni(dmit)$_2$ slabs in α-(EDTTTF)[Ni(dmit)$_2$] is a half and half mixing of these two bands. In addition, as can be realized from figure 14, the intended Ψ^{-}_{HOMO} band is dispersive along both the intrachain ($\Gamma \rightarrow$ Y) and interchain ($\Gamma \rightarrow$ X) directions and thus is a 2D band. In contrast, the intended Ψ^{+}_{LUMO} band is more dispersive along the intrachain than along the interchain direction and thus is a pseudo-1D band. Consequently, since the partially filled band results from the weak hybridization of a 2D and a pseudo-1D band, for many electron transfers the Fermi surface will contain both open and closed components. This is clearly seen in the Fermi surface for $\rho = \frac{1}{2}$ shown in figure 15(a). The Fermi surfaces for the acceptor slabs of α-(EDTTTF)[Ni(dmit)$_2$] are then very different from those of the acceptor slabs of (EDTTTF)$_2$[Pd(dmit)$_2$]$_2$. By contrast, the band structures of the EDTTTF slabs of the two salts

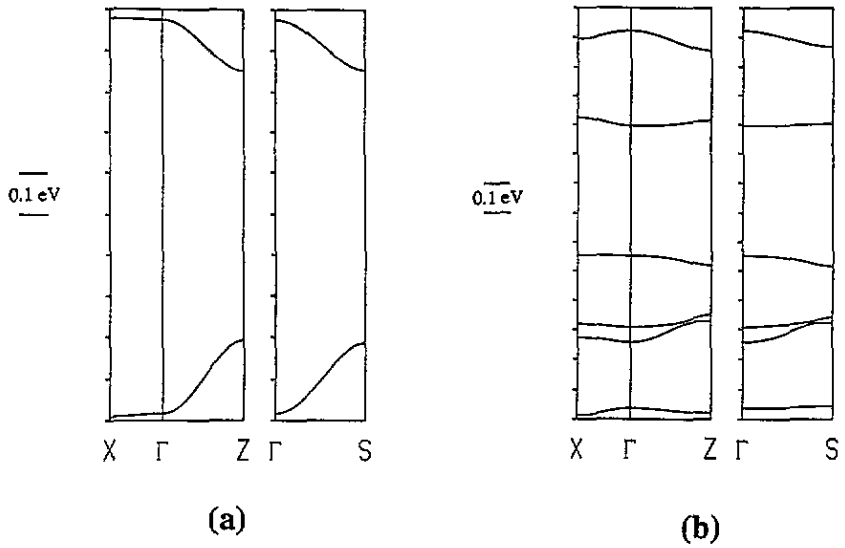

Figure 11. Dispersion relations calculated for the HOMO bands of the EDTTTF slabs (a) and the HOMO and LUMO bands of the Pd(dmit)$_2$ slabs (b) in (EDTTTF)$_2$[Pd(dmit)$_2$]$_3$. Γ, X, Z and S refer to the wavevectors (0, 0), ($a^*/2$, 0), (0, $c^*/2$) and ($-a^*/2$, $c^*/2$), respectively.

are very similar. The calculated Fermi surfaces for the donor slabs of α-(EDTTTF)[Ni(dmit)$_2$] are closed for small electron transfers, become open for larger electron transfers and close again for higher electron transfers. The Fermi surface for $\rho = \frac{1}{2}$ is shown in figure 15(b). The only difference between the EDTTTF Fermi surfaces of the two salts is the range of electron transfers for which these surfaces are open: 0.45–0.65 for α-(EDTTTF)[Ni(dmit)$_2$] and 0.6–0.8 for (EDTTTF)$_2$[Pd(dmit)$_2$]$_2$. With all these results in mind it is quite obvious that the similar resistivity anomalies of (EDTTTF)$_2$[Pd(dmit)$_2$]$_2$ and α-(EDTTTF)[Ni(dmit)$_2$] should be related to some electronic instability of the EDTTTF slabs. At this point we must turn our attention to the temperature dependence of transport, magnetic and structural properties of (EDTTTF)$_2$ [Pd(dmit)$_2$]$_2$.

5. Transport and magnetic properties

5.1. Conductivity measurements

5.1.1. Experimental details. Four-probe conductivity measurements were carried out using a Krohn Hite alternating current source (77 Hz) and a lock-in detector PAR model 5208. Evaporated gold pads were deposited on the crystal before sticking the four gold wires ($d = 17$ μm) with silver paint (Dupont de Nemours).

5.1.2. (EDTTTF)$_2$[Pd(dmit)$_2$]$_3$. The conductivity was measured by the four-probe method on the same crystal used for x-ray structure determination. The room-temperature conductivity is quite high, $\sigma_{RT} = 120$ S cm^{-1}; unfortunately the temperature dependent electrical behaviour could not be determined (the crystal broke upon cooling). No other single crystal of this phase could be obtained to complete the electrical measurements.

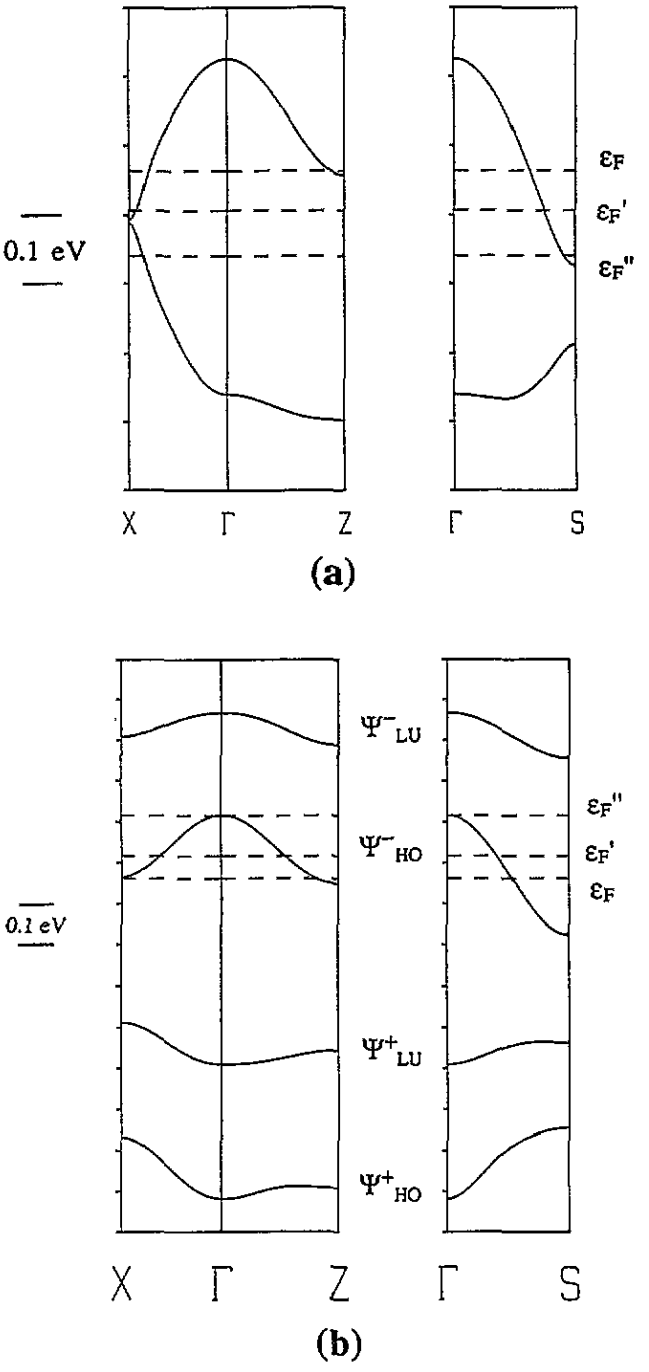

Figure 12. Dispersion relations calculated for the HOMO bands of the EDTTTF slabs (a) and the HOMO and LUMO bands of the $Pd(dmit)_2$ slabs (b) in $(EDTTTF)_2[Pd(dmit)_2]_2$. The Fermi levels denoted ε_F, ε_F' and ε_F'' are those appropriate for charge transfers of $\frac{1}{2}$, $\frac{3}{4}$ and one electrons per molecule. Γ, X, Z and S refer to the wavevectors (0, 0), $(a^*/2, 0)$, $(0, c^*/2)$ and $(-a^*/2, c^*/2)$, respectively.

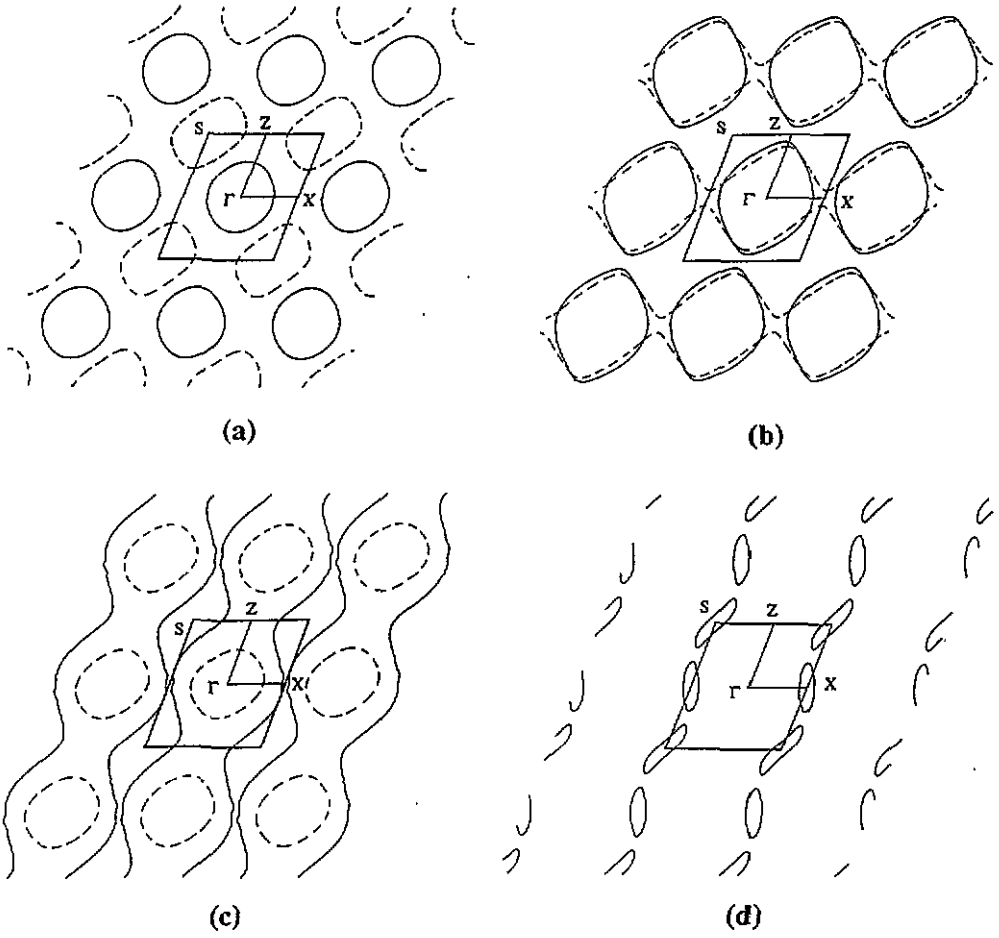

Figure 13. Fermi surfaces for the EDTTTF (full lines) and Pd(dmit)$_2$ slabs (dashed lines) of (EDTTTF)$_2$[Pd(dmit)$_2$]$_2$ calculated assuming a charge transfer of $\frac{1}{4}$ (a), $\frac{1}{2}$ (b), $\frac{3}{4}$ (c) and one (d) electrons per molecule.

5.1.3. (EDTTTF)$_2$[Pd(dmit)$_2$]$_2$. The electrical behaviour of (EDTTTF)$_2$[Pd(dmit)$_2$]$_2$ has been discussed in a previous paper [10] and compared with that of α-(EDTTTF)[Ni(dmit)$_2$]. Let us just recall that under ambient pressure both compounds remain metallic down to very low temperature. A resistivity hump, observed in both cases at 50 K and 15 K respectively, has been assigned to charge density wave instabilities. In order to check this assertion, low-temperature X-ray diffuse scattering experiments were undertaken (see section 6).

5.2. SQUID measurements of (EDTTTF)$_2$[Pd(dmit)$_2$]$_2$

5.2.1. Experimental details. The magnetic susceptibility χ_{meas} was measured in a field of 2 T and every 2 K from 300 to 4 K, using a Quantum Design MPMS SQUID magnetometer. 150 or so, black and shiny platelet-like crystals, of mass 2.60 mg, were mounted inside a very flat sample holder, home machined from a commercial rod of polychlorotrifluoroethylene (PCTFE). In order to get the molar χ_{meas} of the crystals, the diamagnetism [30] of this sample holder was subtracted from the measurements performed in the same conditions on

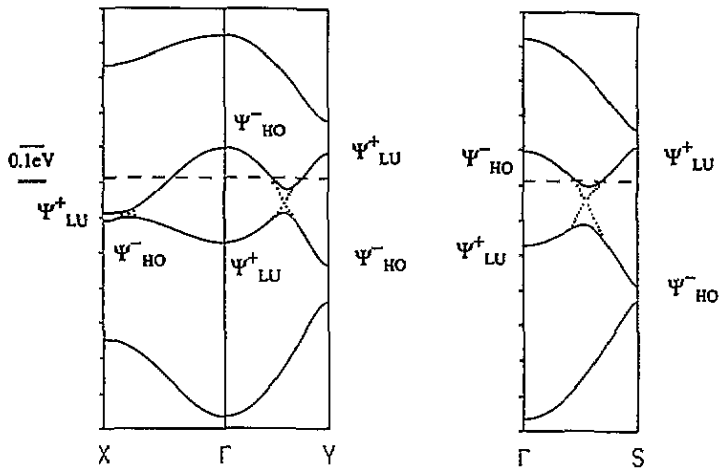

Figure 14. Dispersion relations calculated for the HOMO and LUMO bands of the Ni(dmit)$_2$ slabs in α-(EDTTTF)[Ni(dmit)$_2$]. The dashed line refers to the Fermi level for a charge transfer of $\frac{1}{2}$ electron per molecule. Γ, X, Y and S refer to the wavevectors (0, 0), $(a^*/2, 0)$, $(0, b^*/2)$ and $(-a^*/2, b^*/2)$, respectively.

the material. Care was taken to pump conveniently the airlock access of the experimental chamber in order to remove oxygen, any presence of which, in the vicinity of the sample holder, is reported by a jump of χ especially around 50 K. It has been checked, at 5 K, 10 K and 20 K, that the susceptibility of the crystals plus the sample holder was not field dependent up to 4 T.

5.2.2. Results Figure 16 displays the temperature dependence of the molar static spin susceptibility χ_s of the studied crystals. χ_s has been obtained from the molar χ_{meas} following $\chi_{meas} = \chi_{dia} + \chi_s + C/T$. The diamagnetic contribution χ_{dia} of the elements has been estimated from Pascal's constants [31]. In order to be consistent with a previous study [32] performed upon (TTF)[M(dmit)$_2$]$_2$ with M = Ni or Pd, the C = C constitutive corrections have not been taken into account. Hence χ_{dia} can be evaluated to -7.33×10^{-4} cgs mol^{-1}. Below 40 K appears a Curie tail, which is the signature of paramagnetic impurities. A linear regression of $(T\chi_{meas})$ against T gives a Curie constant C equal to 7.2×10^{-4}cgs K mol^{-1}. This corresponds to 0.2% of free spin-$\frac{1}{2}$ impurities per formula unit, a value which is very similar to that measured [32] in (TTF)[Ni(dmit)$_2$]$_2$. χ_s jumps by a factor of two between 45 and 50 K, about the temperature at which a resistivity hump and a structural modulation (see section 6) are observed. Above 50 K χ_s is temperature independent as expected from a standard Pauli-like behaviour ($\chi_p = 3.7 \times 10^{-4}$ cgs mol^{-1}). Below 45 K χ_s is also temperature independent, in agreement with transport measurements showing that (EDTTTF)$_2$[Pd(dmit)$_2$]$_2$ retains its metallic character. However, the decrease of χ_p by a factor of two suggests that about 50% of the density of states at the Fermi level is removed at the phase transition, the origin of which will be discussed in section 7.

6. Low-temperature x-ray scattering investigation of (EDTTTF)$_2$[Pd(dmit)$_2$]$_2$

As in previous studies of structural instabilities of organic conductors [12], the experiment has been performed with the so-called fixed film–fixed crystal method, using a monochromatized Cu Kα ($\lambda = 1.542$ Å) x-ray beam as incident radiation. Temperatures

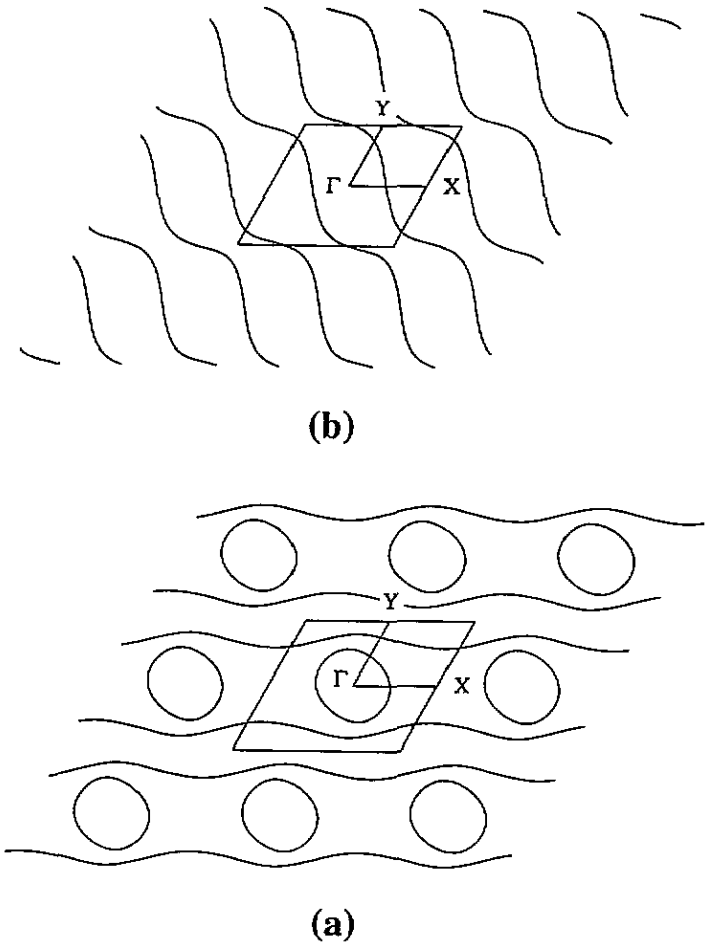

Figure 15. Fermi surfaces for the Ni(dmit)$_2$ (a) and EDTTTF slabs (b) of α-(EDTTTF)[Ni(dmit)$_2$] calculated assuming a charge transfer of $\frac{1}{2}$ electron per molecule.

regulated in the range from 25 K to room temperature were obtained with a closed-circuit cryostat. A single crystal of (EDTTTF)$_2$[Pd(dmit)$_2$]$_2$ having a needle shape (2 mm long and few tenths of a mm of thickness) was glued to the sample holder in good thermal contact with the cold finger of the cryocooler. The sample was oriented with respect to the incoming x-ray beam in such a way that the (a^*, c^*) reciprocal plane, associated to the (010) slabs of identical molecules, was projected on the photographic film.

Evidence for a low-temperature structural distortion is given by the x-ray pattern shown in figure 17. This x-ray pattern, taken at about 25 K, shows (black arrows) supplementary sharp Bragg reflections of very weak intensity. Such weak reflections vanish into a broad diffuse scattering upon heating above a critical temperature T_c estimated at 45 ± 5 K. About 10 superlattice spots are observable on the x-ray pattern of figure 17. They can be indexed by the commensurate reduced critical wave vector $q_c = a^*/4 + c^*/2$ in the (a^*, c^*) reciprocal plane. Their b^* component has not been determined.

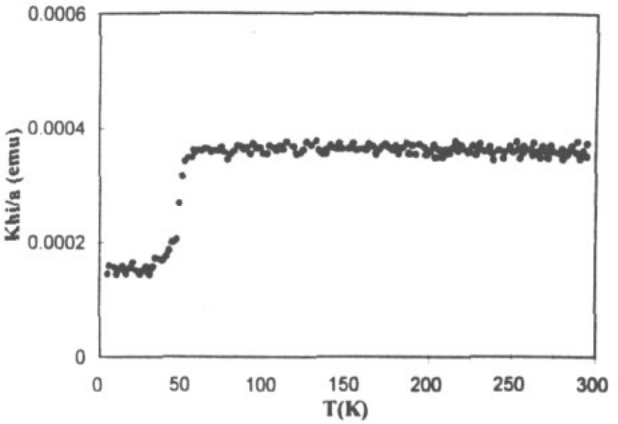

Figure 16. Temperature dependence of the molar static spin susceptibility of single crystals of (EDTTTF)$_2$(Pd(dmit)$_2$)^2. The magnetic field (2 T) was perpendicular to the plane of the platelets.

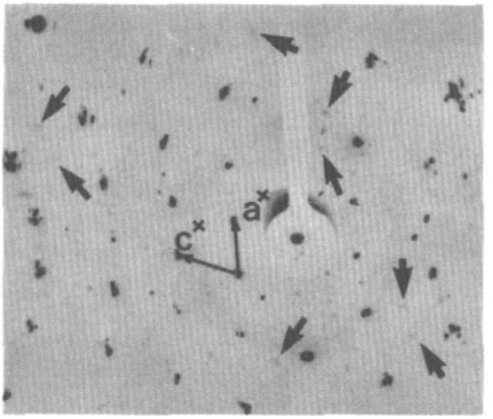

Figure 17. X-ray pattern of (EDTTTF)$_2$[Pd(dmit)$_2$]$_2$ at 25 K showing (black arrows) the q_c superlattice spots. The a^* and c^* reciprocal directions are indicated.

7. Discussion

The two charge transfer salts (EDTTTF)$_2$[Pd(dmit)$_2$]$_2$ and α-(EDTTTF)[Ni(dmit)$_2$] have similar crystal structures and resistivity anomalies. However, our study of the correlation between their crystal and electronic structures shows that this similarity is only partial. The difference in the dimerization degree of the M(dmit)$_2$ slabs, i.e., absence of dimerization in α-(EDTTTF)[Ni(dmit)$_2$] but strong dimerization in (EDTTTF)$_2$[Pd(dmit)$_2$]$_2$, leads to a completely different electronic structure for the acceptor slabs of the two salts. Thus, the partially filled band of the acceptor slabs of (EDTTTF)$_2$[Pd(dmit)$_2$]$_2$ is built from the Ψ^-_{HOMO} orbital whereas that of α-(EDTTTF)[Ni(dmit)$_2$] is built from a half and half mixing of the Ψ^-_{HOMO} and Ψ^+_{LUMO} orbitals. This leads to Fermi surfaces which are quite different. In contrast, the electronic structures of the donor slabs of the two salts are very similar. In view of the similarity of the resistivity anomalies of the two salts we conclude that the EDTTTF donor slabs are at the origin of the resistivity anomalies. Analysis of the transverse magnetoresistance in α-(EDTTTF)[Ni(dmit)$_2$] [33] led to the same conclusion for this salt. However, our study allows us to go a step further in understanding the physical behaviour of these salts.

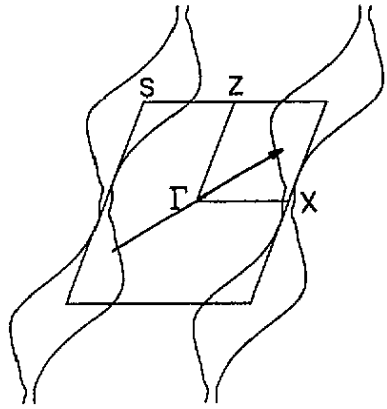

Figure 18. Fermi surface for the EDTTTF slabs of (EDTTTF)$_2$[Pd(dmit)$_2$]$_2$ calculated assuming a charge transfer of $\frac{3}{4}$ electrons per molecule. The critical CDW wave vector q' is also shown.

The strong reduction of the magnetic spin susceptibility at the onset of the resistivity hump, and at the same temperature at which superlattice spots can be detected in the x-ray patterns of (EDTTTF)$_2$[Pd(dmit)$_2$]$_2$, clearly prove that this salt undergoes a charge density wave (CDW) structural transition at about T_c = 40–50 K. Such features which affect both the charge and spin degrees of freedom are expected from a regular Peierls mechanism. However as the metallic state is retained below T_c with only a reduction of 50% of the density of state, only a partial gap opening is achieved by the CDW–Peierls transition in the conduction band structure at the Fermi level. In order to understand more deeply the origin of this CDW transition we need to compare the experimentally determined critical wave vector q_c with the possible nesting vectors of our calculated Fermi surfaces as a function of ρ. In addition this will lead us to determine the approximate charge transfer ρ for this salt. The best agreement occurs for the Fermi surface of EDTTTF calculated for a charge transfer of 0.75 where, as shown in figure 18, the $a^* + c^* - q_c = \frac{3}{4}a^* + c^*/2 = q'$ wave vector nests a large part of its flat portions. In this respect it is interesting to remark that the value 0.75 of the charge transfer ρ of (EDTTTF)$_2$[Pd(dmit)$_2$]$_2$ is comparable to that suggested [16, 17] in (TTF)[Pd(dmit)$_2$]$_2$.

What is the physical meaning of these results? The warped lines of the 1D Fermi surface of figure 18 are perpendicular to the a direction which, as mentioned, is the direction along which the EDTTTF donors pile up. Given the quasi-1D character of the Fermi surface, the a^* component of q' should correspond to the $2k_F$ wave vector. Since the stack contains dimer units, its value (3/4) corresponds to the charge transfer which, consistently, coincides with the value used to calculate the Fermi surface. The $c^*/2$ component means that the CDW modulations are out of phase between successive chains of the EDTTTF donor slabs, probably in order to minimize the Coulomb interactions. At this point it is interesting to note that the best nesting wave vector for the Fermi surface of figure 18 is $\frac{3}{4}a^* + 0.58c^*$, i.e., the transverse component is slightly different from the observed one. This means that there is a competition between the Coulomb interactions, which tend to impose the commensurate value 0.5 c^*, and the interchain overlap interactions, which tend to impose the incommensurate value 0.58 c^*. Clearly, the interchain Coulomb interactions dominate over the interchain transfer integrals.

Our conclusion is that only the donor stacks of (EDTTTF)$_2$[Pd(dmit)$_2$]$_2$ undergo a Peierls transition, a feature which qualitatively explains the drop of 50% of the density of states at

the Fermi level below T_c.

The similarity of the resistivity humps, the magnetoresistance study by Tajima *et al* [33] and the theoretical study of section 4 suggest that the resistivity anomaly of α-(EDTTTF)[Ni(dmit)$_2$] should also be associated with a CDW instability of the EDTTTF slabs. According to our calculations, the best nesting wave vector for the EDTTTF slabs of this salt is found for the Fermi surface calculated for a charge transfer of $\frac{1}{2}$ (see figure 15(b)) where the nesting wave vector $a^*/2$ is readily apparent. Let us remind that the EDTTTF molecules pile up along the $(a+b)$ direction in this salt so that the modulation wave vector should have a component of $\frac{1}{2}$ along both the chain and the interchain directions. Thus in that case the Coulomb and overlap effects tend to impose the same value for the transverse component. X-ray diffuse scattering measurements would be very interesting in order to establish that a CDW instability is also at the origin of the resistivity hump in α-(EDTTTF)[Ni(dmit)$_2$] and that the charge transfer in this salt is around $\frac{1}{2}$.

8. Concluding remarks

Two new M(dmit)$_2$ charge transfer salts, (EDTTTF)$_2$[Pd(dmit)$_2$]$_2$ and (EDTTTF)$_2$[Pd(dmit)$_2$]$_3$, have been prepared and characterized. (EDTTTF)$_2$[Pd(dmit)$_2$]$_2$ is a metallic charge transfer salt exhibiting a resistivity anomaly at 50 K. Analysis of the crystal and electronic structures of this salt as well as transport, magnetic and x-ray diffuse scattering measurements clearly establish that this anomaly originates from a CDW modulation of the donor slabs and suggest that the charge transfer in this salt is of $\frac{3}{4}$ electrons per molecule. Our study also suggests that the resistivity anomaly of the related salt α-(EDTTTF)[Ni(dmit)$_2$] is due to a CDW instability of the donor slabs although the charge transfer is smaller ($\rho = \frac{1}{2}$). (EDTTTF)$_2$[Pd(dmit)$_2$]$_3$ contains real [Pd(dmit)$_2$]$_3$ trimeric units and exhibits a quite high room temperature conductivity. Our study suggests a charge transfer of one electron per EDTTTF molecule and that the resistivity–temperature behaviour of this salt should be of the semiconducting type.

References

[1] Williams J M, Ferraro J R, Thorn R J, Carlson K D, Geiser U, Wang H H, Kini A M and Whangbo M-H 1992 *Organic Superconductors* ed R N Grimes (Englewood Cliffs, NJ: Prentice-Hall)

[2] Kikuchi K, Murata K, Honda Y, Namiki T, Saito K, Anzai H, Kobayashi K, Ishiguro T and Ikemoto I 1987 *J. Phys. Soc. Japan.* **56** 4241–44 and references therein

[3] Papavassiliou G C, Mousdis G A, Zambounis J S, Terzis A, Hountas A, Hilti B, Mayer C W and Pfeiffer J 1988 *Synth. Met.* B **27** 379–83

[4] Papavassiliou G C, Mousdis G A, Kakoussis V C, Terzis A, Hountas A, Hilti B, Mayer C W and Zambounis J S 1990 *The Physics and Chemistry of Organic Superconductors* vol 51, ed G Saito and S Kagoshima (Berlin: Springer) pp 247–50
Biberacher W, Muller H, Heidmann C-P, Probst C, Lerf A, Andres K, Kakoussis V C, Papavassiliou G C, Mousdis G A, Riede J and Hummel H U 1991 *Synth. Met.* **42** 2377–80

[5] Kato R, Kobayashi H and Kobayashi A 1989 *Chem. Lett.* 781–84
Kobayashi A, Kato R and Kobayashi H 1990 *The Physics and Chemistry of Organic Superconductors* vol 51, ed G Saito and S Kagoshima (Berlin: Springer) pp 302–5

[6] Cassoux P, Valade L, Kobayashi H, Kobayashi A, Clark R A and Underhill A E 1991 *Coord. Chem. Rev.* **110** 115–60 and references therein

[7] Kato R, Kobayashi H, Kobayashi A, Naito T, Tamura M, Tajima H and Kuroda H 1989 *Chem. Lett.* 1839–42

[8] Tajima H, Inokuchi M, Kobayashi A, Ohta T, Kato R, Kobayashi H and Kuroda H 1993 *Chem. Lett.* 1235–38

[9] Garreau B, Pomarède B, Faulmann C, Fabre J-M, Cassoux P and Legros J-P 1991 *C. R. Acad. Sci., Paris* II **313** 509–16

[10] Brossard L, Ribault M, Garreau B, Pomarède B and Cassoux P 1992 *Europhys. Lett.* **19** 223–7

[11] Pomarède B, Garreau B, Malfant I, Valade L, Cassoux P, Legros J- P, Audouard A, Brossard L, Ulmet J-P, Doublet M-L and Canadell E 1994 *Inorg. Chem.* **33** 3401–14
[12] Underhill A E, Clark R A, Marsden I, Allan M, Friend R H, Tajima H, Naito T, Tamura M, Kuroda H, Kobayashi A, Kobayashi H, Canadell E, Ravy S and Pouget J-P 1991 *J. Phys.: Condens Matter* **3** 933–54
[13] Ravy S, Canadell E, Pouget J-P, Cassoux P and Underhill A E 1991 *Synth. Met.* **42** 2191–4
[14] Canadell E, Ravy S, Pouget J-P and Brossard L 1990 *Solid State Commun.* **75** 633–8
[15] Brossard L, Ribault M, Valade L and Cassoux P 1989 *J. Physique* **50** 1521–34
Brossard L, Ribault M, Valade L and Cassoux P 1990 *Phys. Rev.* B **42** 3935–43
[16] Ravy S, Canadell E and Pouget J-P 1990 *The Physics and Chemistry of Organic Superconductors* vol 51, ed G Saito and S Kagoshima (Berlin: Springer) pp 252–6
[17] Canadell E, Rachidi E I, Ravy S, Pouget J-P, Brossard L and Legros J-P 1989 *J. Physique* **50** 2967–81
[18] Ravy S, Pouget J-P, Valade L and Legros J-P 1989 *Europhys. Lett.* **9** 391–6
[19] Brossard L, Ribault M, Doublet M-L, Canadell E, Garreau B and Legros J-P 1993 *Synth. Met.* **56** 2833–8
[20] Sheldrick G M 1986 *SHELX 86 Program for Crystal Structure Solution* (Göttingen: University of Göttingen)
[21] Fair C K 1990 *MolEN Structure Determination System* (Delft: Enraf-Nonius)
[22] Garreau B 1993 *Thèse d'Université* Toulouse
Garreau B, De Montauzon D, Cassoux P, Legros J-P, Fabre J-M, Saoud K and Chakroune S 1995 *New J. Chem.* **19** 161–71
[23] Legros J-P, Valade L and Cassoux P 1988 *Synth. Met.* B **27** 347–52
[24] Kobayashi A, Kobayashi H, Miyamoto A, Kato R, Clark R A and Underhill A E 1991 *Chem. Lett.* 2163–6
[25] Kobayashi A, Kato R, Clark R A, Underhill A E, Miyamoto A, Bun K, Naito T and Kobayashi H 1993 *Synth. Met.* **56** 2927–32
Kobayashi H, Bun K, Naito T, Kato R and Kobayashi A 1992 *Chem. Lett.* 1909–12
[26] Whangbo M-H, Hoffmann R 1978 *J. Am. Chem. Soc.* **100** 6093–8
[27] Ammeter J, Bürgi, H-B, Thibeault J, Hoffmann R 1978 *J. Am. Chem. Soc.* **100** 3686–92
[28] Whangbo M-H, Williams J M, Leung P C W, Beno M A, Emge T J and Wang H H 1985 *Inorg. Chem.* **24** 3500–2
Williams J M, Wang H H, Emge T J, Geiser U, Beno M A, Leung P C W, Carlson K D, Thorn R J, Schultz A J and Whangbo M-H 1987 *Prog. Inorg. Chem.* **35** 51–218
Since overlap is explicitly included in extended Hückel calculations, these interaction energies (β) should not be confused with the conventional transfer integrals (t). Although the two quantities are obviously related and have the same physical meaning, the absolute values of β are somewhat greater than those of t.
[29] Doublet M-L 1994 *Thèse d'Université* Orsay
[30] Mari A and Brossard L 1993 *Rev. Sci. Instrum.* **64** 1364
[31] Figgis B N and Lewis J 1960 *The Magnetochemistry of Complex Compounds, in Modern Coordination Chemistry* ed J Lewis and R G Wilkins (New York: Interscience).
Values of Pascal's constants (in units of 10^{-6} cgs mol^{-1}): H, 2.93; C, 6.00; S, 15.0; Pd^{2+}, 25.0.
[32] Brossard L, Canadell E, Valade L and Cassoux P 1993 *Phys. Rev.* B **47** 1647–50
[33] Tajima H, Ikeda S, Kobayashi A, Kuroda H, Kato R and Kobayashi H 1993 *Synth. Met.* **56** 2323–8